Measurement of t_{20} in $\pi^+ d$ elastic scattering

N. R. Stevenson,* Y. M. Shin, K. Itoh, and G. Retzlaff†
University of Saskatchewan, Saskatoon, Saskatchewan, Canada S7N 0W0

D. R. Gill, D. F. Ottewell, and G. D. Wait
TRIUMF, Vancouver, British Columbia, Canada V6T 2A3

T. E. Drake, D. Frekers,* and R. B. Schubank‡
University of Toronto, Toronto, Ontario, Canada M5S 1A7

G. J. Lolos
University of Regina, Regina, Saskatchewan, Canada S4S 0A2
(Received 9 March 1988; revised manuscript received 14 December 1988)

Measurements of the tensor polarization t_{20} in $\pi^+ d$ elastic scattering have been performed at $\theta_d^{\rm lab}=15°$ between $T_\pi=116$ and 145 MeV. Angular distributions at 133 and 140 MeV were also determined. These results resolve the discrepancy that has existed between the measurements made by other groups at SIN and at LAMPF, as our values are negative for all energies and angles investigated and consistent with the LAMPF data. Our results are also in good agreement with the corresponding measurements of analyzing powers. Lack of any significant oscillatory nature is in general agreement with theories at these kinematic regions and does not lend support to exotic effects such as dibaryon resonances.

I. INTRODUCTION

The study of the $\pi d(\pi NN)$ system is of fundamental importance in understanding the pion nucleus interaction and for investigation of the role of quarks in nuclei. It is the only three-body system which can, in principle, be calculated exactly, and comparisons with experimental data can be used to find deficiencies in theory.

In recent years, the πd elastic system has been studied quite extensively. The elastic differential cross section has been measured precisely[1] up to $T_\pi=300$ MeV, in addition to some polarization observables.[2] The first measurement of the tensor polarization, t_{20}, of the recoil deuterons in πd elastic scattering was performed by Holt *et al.*[3,4] and subsequently by Ungricht *et al.*[5,6] at the Clinton P. Anderson Meson Physics Facility (LAMPF). Other measurements at the Swiss Institute for Nuclear Research (SIN) followed by Ulbricht *et al.*,[7] Grüebler *et al.*,[8] and König *et al.*[9] The measurements carried out at LAMPF and SIN have shown a vast difference. The results of the former showed that t_{20} is negative and varies smoothly with energy and angle while that of the latter indicated that it is positive and varies rapidly over the same energy and angular range ($120 \le T_\pi \le 150$ MeV; $15° \le \theta_d^{\rm lab} \le 45°$).

In a subsequent measurement at TRIUMF[10] we have shown that t_{20} is negative and a smooth function of both angle and energy in agreement with the LAMPF group. More recently, the tensor analyzing power, T_{20}, has been measured by Smith *et al.*[11] The results are in good agreement with Shin *et al.*[10] and the LAMPF group,[3–6] and eliminate the need for exotic effects such as dibaryon resonances which were claimed by the group who measured t_{20} at SIN.[9]

Theoretical calculations[12–24] based on the Faddeev method have reached a high level of sophistication. Comparisons with experimental results have shown that most theoretical calculations predict the gross features of πd elastic scattering. Although discrepancies between theory and experiment have existed in the differential cross section and vector analyzing power (iT_{11}), it was the measurements of t_{20} which have shown, through comparison with theory, that at least for t_{20}, the discrepancy stems from the inadequate treatments of the $\pi N P_{11}$ intermediate interaction, or the true pion absorption mechanism. Such a comparison between theory and experiment often yields details of physical processes involved in the reaction, but the ultimate quantities of interest to theory are the unambiguous determination of partial-wave amplitudes/phase shifts for which a complete set of experimental data are needed. At present a limited set of data on πd elastic scattering are available and only the largest few partial-wave amplitudes have been determined with reasonable certainty.[25] In order to obtain all amplitudes unambiguously, polarization transfer coefficients in addition to the existing data need to be determined. To measure such polarization observables requires a suitable polarimeter to analyze the recoil deuterons. One of the aims of this paper is to clarify the confusion that has arisen from the discrepancies in the *polarization* measurements of πd elastic scattering.

It is very difficult to pinpoint the sources of the error that lead to the experimental discrepancies mentioned previously. However, if sufficient diagnostic tools are in-

stalled in an experiment, such as in the arrangement we describe here, it is possible to conjecture the most probable sources of the errors.

In this paper we present the details of the measurement of the tensor polarization t_{20} of the recoil deuterons in πd elastic scattering between $T_\pi = 116$ and 145 MeV and angular distribution at 133 and 140 MeV. A summary of this study has been reported earlier.[10] In view of the importance of the further application of a polarimeter, a detailed description of the experiment (Sec. II) and analysis (Sec. III) are given. In Sec. IV we discuss the experimental results comparing with theory, and make a critical assessment of the experiment. Finally, conclusions are drawn from our study in Sec. V.

II. EXPERIMENTAL DETAILS

The measurements were performed at TRIUMF in the upgraded $M11$ pion channel. Positive pions with a flux of $1 \sim 4 \times 10^7$ s^{-1}($\Delta p/p = 2 \sim 5\%$) were used. The beamline momentum was known to ± 0.7 MeV/c. It had been calibrated[26] by measuring the energy of various ions (p^+, d^+, t^+, $^3He^{++}$, and $^4He^{++}$) from the production target with solid-state detectors and, in addition, by determining the time-of-flight (TOF) difference between pions and protons through the channel. After the momentum calibration, a midstream absorption plate (2.1-mm CH_2) in the $M11$ channel ensured that other stray charged particles (protons, etc.,) were removed from the pion beam. The momentum spread and intensity of the channel were controlled by pairs of slits and jaws positioned in the front end and center of the $M11$ channel.

Measurements of the spatial and angular extent of the beam at the achromatic focal point are shown in Fig. 1. Typically, the beam measured 1.0 cm horizontally by 1.1-cm FWHM vertically with a divergence of 0.7° and 3.2°, respectively. To determine the relative pion flux and any beam instabilities in the $M11$ channel, the muon "halo" was monitored at the exit window with the use of four small (3.2 cm×3.2 cm×0.3 cm) scintillators ($\mu 1 - \mu 4$) which were arranged in pairs as telescopes, $\mu 1 \cdot \mu 2$ above the beamline and $\mu 3 \cdot \mu 4$ below the beamline.

Figure 2 shows a schematic of our experimental layout in the $M11$ area. A liquid deuterium target (LD_2) was positioned at the achromatic focal point of the channel. The beam profile on the target was measured with a retractable ion integrating wire chamber, $W0$, which was positioned next to the entrance window of the target. This chamber, which had a spatial resolution of ± 1.5 mm both horizontally and vertically, was used before and after each run, and at any point it was interrupted, but was moved out of the beam during the measurement period.

The liquid deuterium target[27] consisted of two isolated identical target cells, mechanically attached one above the other as shown in Fig. 3. One cell contained the liquid deuterium while the other was filled with helium gas and used for the background measurements. The target was a 10-cm-diam and ~ 7.5-mm-thick disk (~ 120

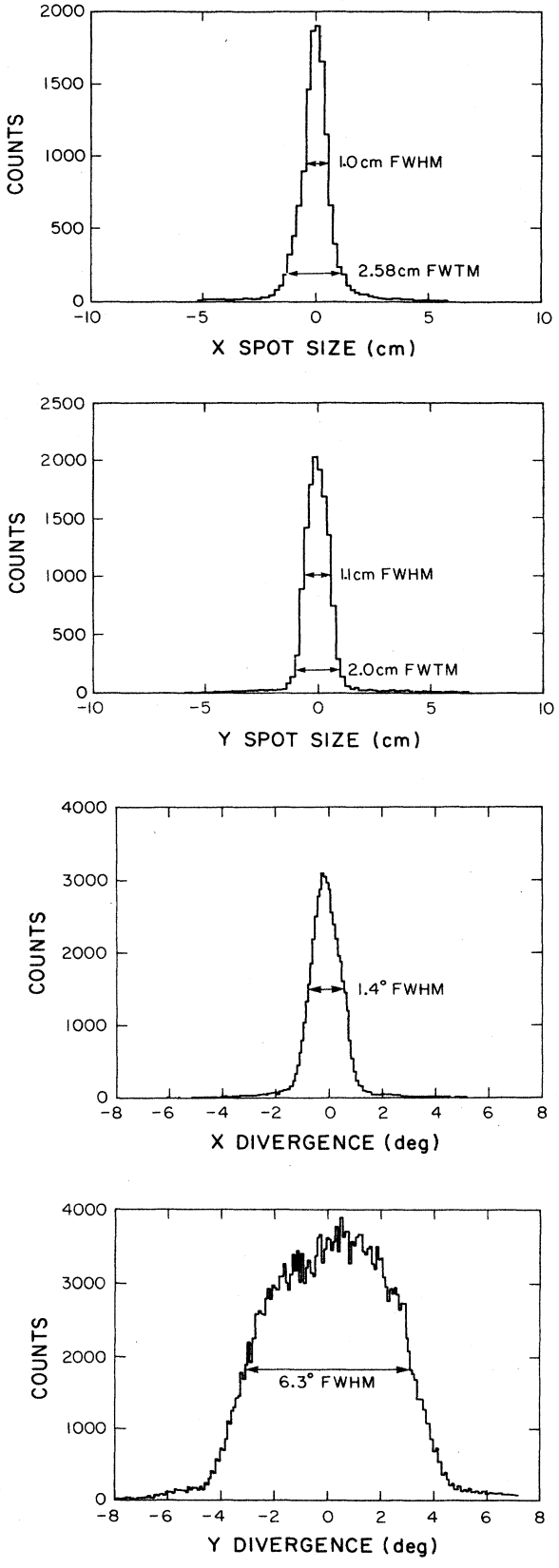

FIG. 1. Beam dimensions at the $M11$ achromatic focus (target) position.

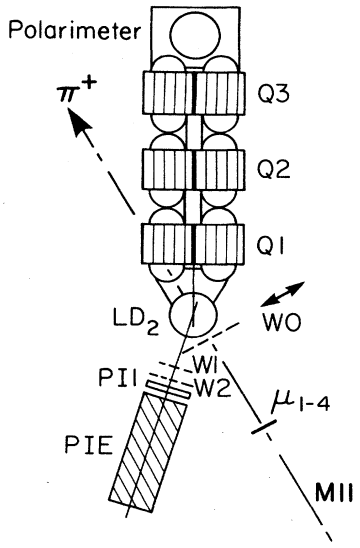

FIG. 2. Experimental configuration at TRIUMF. The beam was monitored in scintillators (μ_{1-4}) and a retractable wire chamber ($W0$). Pions scattered from the liquid deuterium target (LD_2) were detected in wire chambers ($W1, W2$) and scintillators (PI1,PIE). The recoil deuterons were focused by the quadrupole triplet ($Q1$, $Q2$, and $Q3$) onto the polarimeter.

mg cm^{-2} at 20 K) so that the background from the frame was eliminated. Each target cell had 50-μm inner mylar windows (containing the target material) separated from outer 130-μm mylar windows by an $\sim$6.5-mm-thick envelope of ^{4}He gas ($\sim$1.6 mg cm^{-2}). The target cell assemblies were surrounded by five layers of 6-μm aluminized mylar which acted as a heat shield. This inner cell arrangement was contained within the outside vacuum jacket which has two 250-μm-thick mylar windows each of which spanned 125° in the horizontal scattering plane and ±18° vertically. The target was continually monitored by a microprocessor controlled system which kept the operation of the cell to within ±0.1 K of its nominal temperature. For each run the target assembly was rotated such that both scattered pions and recoiling deuterons emerged through the vacuum jacket windows. The inner target cell was so adjusted that the recoil deuterons exited normally from the target cell at the angle under investigation thus minimizing the energy loss and straggling.

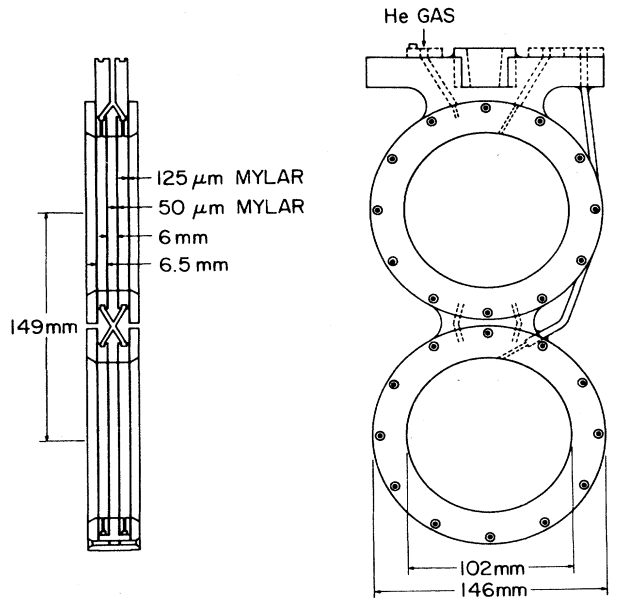

FIG. 3. Details of the liquid deuterium (LD_2) target assembly.

Scattered pions were counted with the pion arm detection system consisting of wire chambers ($W1, W2$) and scintillation counters (PI1, PIE) as shown in Fig. 2. The wire chambers, $W1$ (30 cm×30 cm) and $W2$ (20 cm×20 cm), each has a 2-mm vertical by 0.7-mm horizontal grid resolution and were positioned 62 cm and 85 cm, respectively, from the center of the LD_2 target. The detector system consisted of a large thin (30-cm-diam×0.6-cm-thick) plastic scintillator PI1 for ΔE and a large cylindrical plastic counter PIE, 30 cm in diameter and 45 cm in length, for determining the total energy.

The deuteron arm consisted of a quadrupole triplet and polarimeter. The triplet was used primarily to increase the solid angle (the acceptance was about 125 mrad vertically by 35 mrad horizontally) and to act as a momentum filter. The triplet was operated symmetrically in a V-H-V focusing mode. The properties of this triplet had been carefully examined by a combination of magnetic field maps and computer simulation to obtain optimum focusing characteristics before the experiment. At the initial stage of the measurements the triplet was set to the computed field values and then "fine tuned" by mapping out the deuterons arriving at the polarimeter surface (D counter) to obtain the sharpest spatial distribution of the π events. For each subsequent measurement the operating values of the triplet were scaled according to the central deuteron momentum.

The deuterons that were focused by the triplet entered the polarimeter assembly shown in Fig. 4. At the center of the polarimeter was a cylindrical ^{3}He gas cell 10 cm in diameter and 10 cm long. This cell was surrounded by a jacket of liquid ^{4}He at 4.2 K. The cell windows were composed of 25-μm stainless steel clamped to the cell frame with indium seals. The cell was surrounded by a heat shield composed of four layers of 6-μm aluminized mylar wound about a thin copper frame. Outside of this was the vacuum drum which had 120-μm-thick mylar windows that were 12.7 cm in diameter.

Deuterons entering the polarimeter initially had their energy degraded in a thin copper foil and/or a thin ($\sim$0.8-mm) scintillator ("active absorber"), A, in order to bring the deuteron energies within the calibration range of the polarimeter. Subsequently, they were detected in wire chambers $W3$ and $W4$ which were separated by a drift space of 4 cm to obtain an angular resolution of $\sim$4°. Next, scintillator D, of area 10 cm×10 cm and thickness 0.8 mm, was used to monitor the deuteron flux incident on the polarimeter. The analyzing reaction in

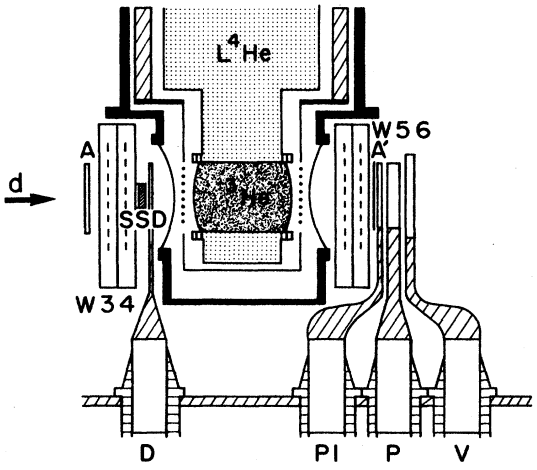

FIG. 4. Polarimeter assembly consisting of a ^{3}He gas cell surrounded by wire chambers ($W3-6$), scintillators (D, P1, P, V), absorbers (A, A') and retractable solid-state detectors (SSD's).

the polarimeter cell was ^{3}He$(d,p)^4$He with the emerging protons being detected spatially by wire chambers $W5$ and $W6$. The ΔE spectrum measured in scintillator P1 (10 cm×10 cm×0.8 mm) and the total energy determined in scintillator P (10 cm×10 cm×1.27 cm) contributed to the detection and determination of the real (d,p) events. A 12.5 cm×12.5 cm×1.27 cm scintillator V, mounted at the end of the polarimeter, vetoed other energetic particles. A 0.25-mm copper absorber A' prevented noninteracting deuterons from entering the proton telescope while allowing the emerging protons, produced by the analyzing reaction. Should any remaining deuterons have reached the proton telescope they would have been identified by examining the ΔE-E signature in P1 and P.

The energy spectra of the impinging deuterons were measured with the use of solid-state detectors (SSD) arrayed in the form of a ΔE-E telescope (1 mm and 4 mm thick) which was capable of measuring up to 50-MeV deuterons with a resolution of $\sim$100 keV. The telescope

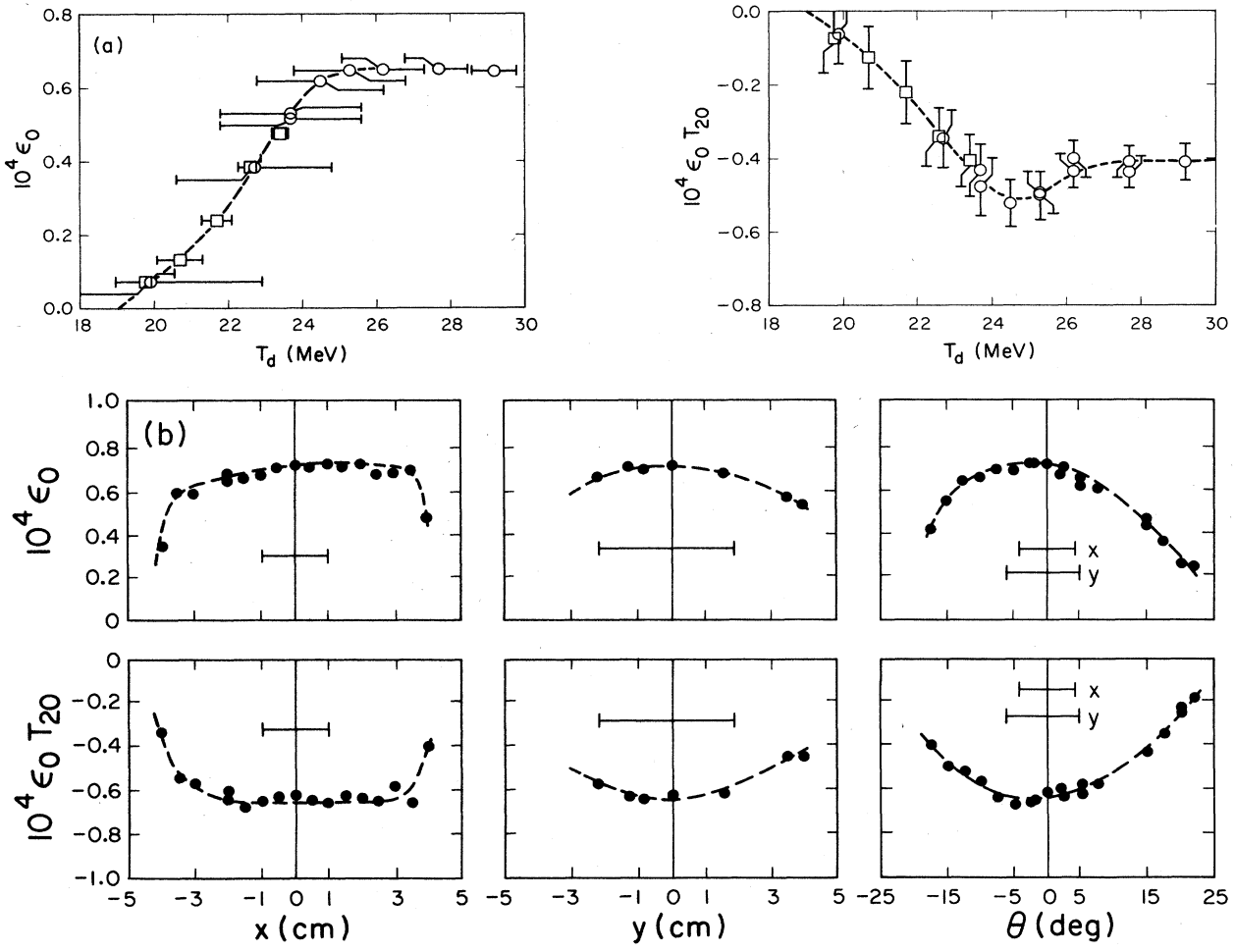

FIG. 5. Calibration curves for the polarimeter (broken lines are drawn to guide the eye). The statistical errors are smaller than the plotted characters. (a) Dependency of ϵ_0 ("error" bars indicate extent of energy distribution after degradation in absorbers) and $\epsilon_0 T_{20}$ (error bars represent uncertainty in polarization) on the incident deuteron energy. (b) Positional and angular dependencies.

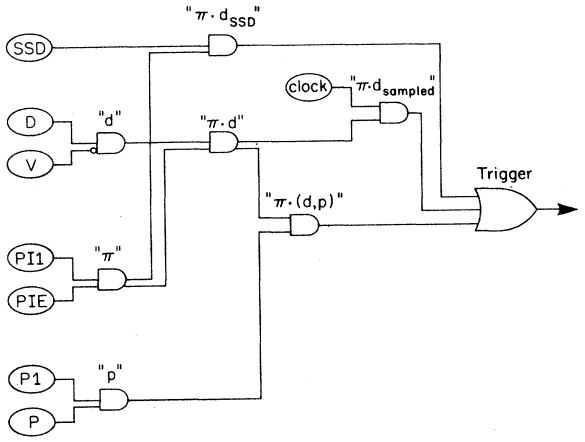

FIG. 6. On-line electronic trigger logic.

temporarily replaced the wire chamber $W4$ before, during, and/or after each of the t_{20} measurements. In this way we measured each deuteron energy distribution directly.

The polarimeter was calibrated with a polarized deuteron beam at the Texas A&M Cyclotron Institute. A detailed description of the polarimeter and the calibration procedure is to be found elsewhere.[28] Briefly, 25- and 35-MeV deuterons with known polarization from the cyclotron were analyzed and focused onto the polarimeter at an intensity of $\leq 10^5$ per second. The energies of deuterons entering the polarimeter were stepped down by the use of appropriate absorbers to study the energy dependence of the efficiency, ϵ_0, and analyzing power, T_{20}. Any possible depolarization effects were studied by comparing the results of the two primary cyclotron energies but none was detected. The position and angle dependences were determined by moving and rotating the polarimeter with respect to the incident beam. The results of the calibration are shown in Figs. 5(a) (energy dependence) and (b) (spatial dependence). Also studied was the dependence on ^{3}He cell gas pressure which was optimized (766 torr) to provide the highest efficiency.

To ensure that the electronic threshold levels and the gains on the D, P1, and P counters were always set in a consistent manner we placed an ^{241}Am source on the corners of each detector. The position of the alpha peak served as a reference point in both the calibration and πd measurements. Another independent method of establishing the correct thresholds and gains was made by comparing 35-MeV deuteron spectra during the calibration with that at TRIUMF (measured with SSD's and supplemented by the TOF spectra).

A simplified electronics schematic of that used at TRIUMF to define events is shown in Fig. 6. The output formed the LAM signal in the CAMAC system which was interfaced to a PDP 11/34 computer. A clock was used for sampling the deuteron spectra. The information registered by the computer included the following.

(1) Pulse height spectra of detectors D (sampled), P1, P, V, PI1, and PIE.

(2) Total number of deuterons detected by the D counter.

(3) TOF spectra between PI1 and D, P1, and P.

(4) Positions of pions, deuterons, and protons as measured by $W1-6$.

(5) All events with $\pi\cdot D\cdot P1\cdot P\cdot\bar{V}$.

The events most frequently registered were protons from the reaction $d(\pi,p\pi')n$ whose cross section is an order of magnitude higher than the elastic reaction. While kinematic constraints reduced these events significantly, a large number of protons strayed into the system (and missed the veto counter) due to the large solid angle ac-

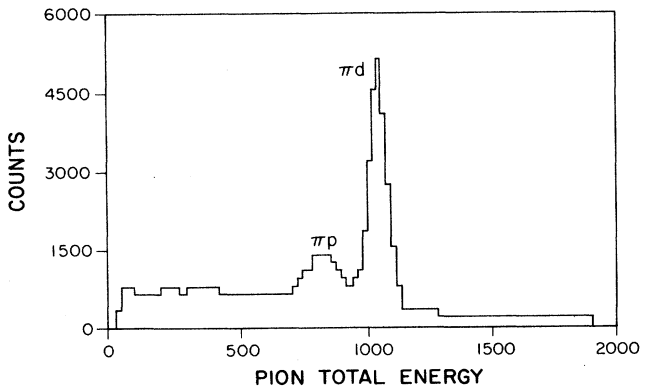

FIG. 7. Scattered pion total energy spectrum (scale is in channel numbers).

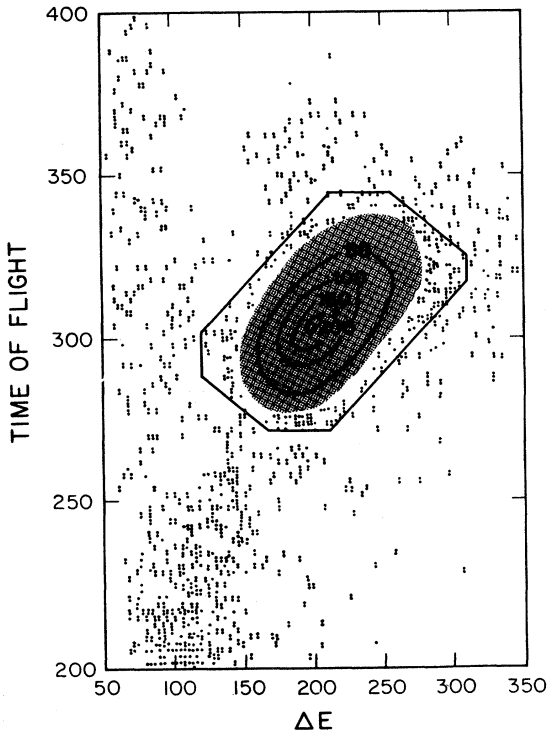

FIG. 8. Identification of deuterons in the D counter during the t_{20} measurements (scales are in channel numbers).

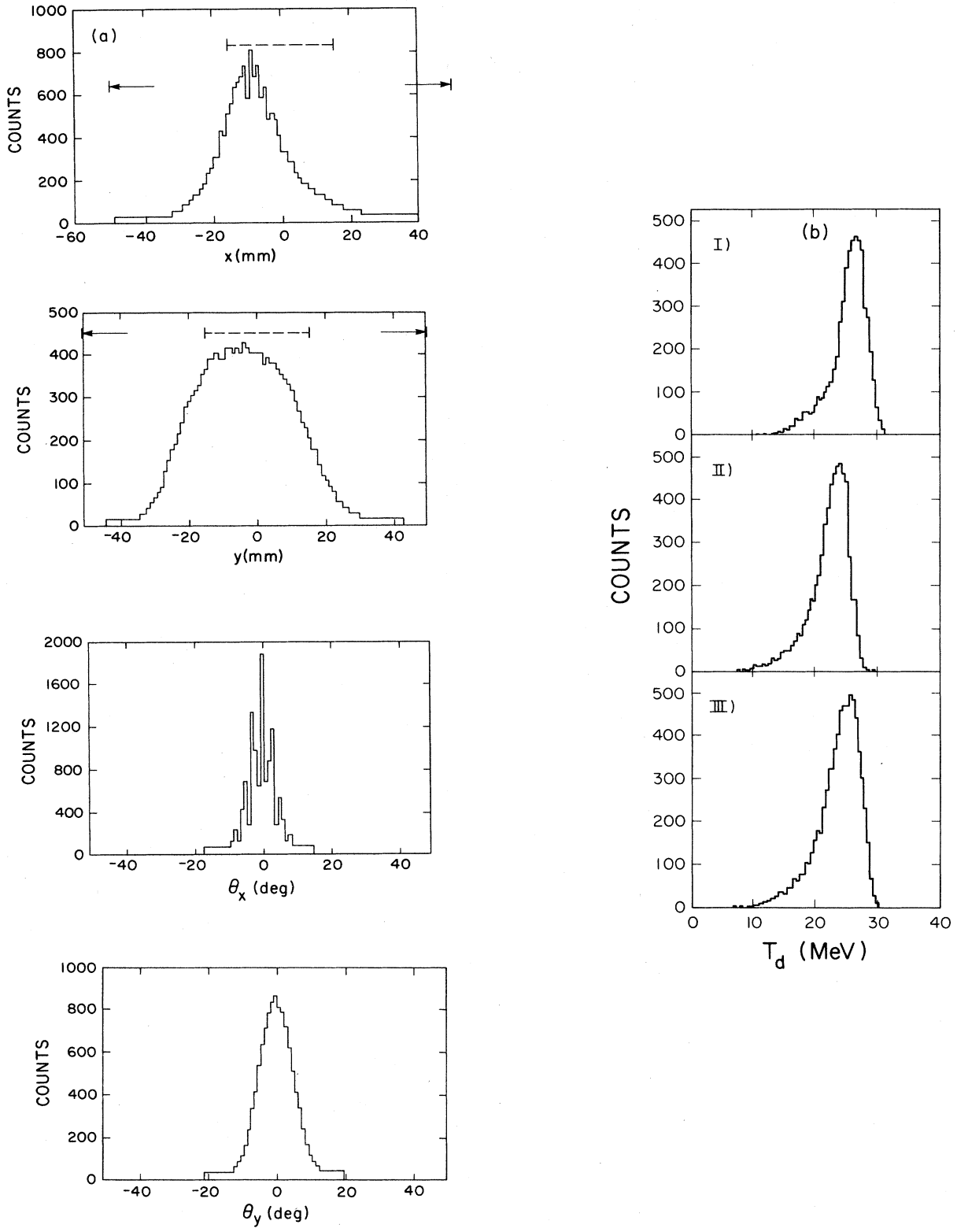

FIG. 9. Deuteron distributions measured at the polarimeter in a typical t_{20} measurement. (a) Spatial and angular distributions. Arrows indicate the dimensions of our polarimeter as compared to that of Ref. 30 (dashed lines). The structure observed in the θ_x distribution arises due to the quantized nature of the wire chambers (2 mm wire spacing in this direction). (b) Energy distributions (I $T_\pi = 133$ MeV/$\theta_\pi = 150°$; II 141 MeV/150°; III 133 MeV/130°).

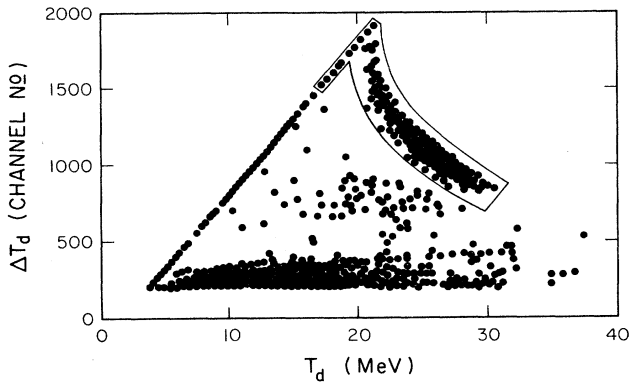

FIG. 10. Identification of deuterons in the solid-state detector measurements.

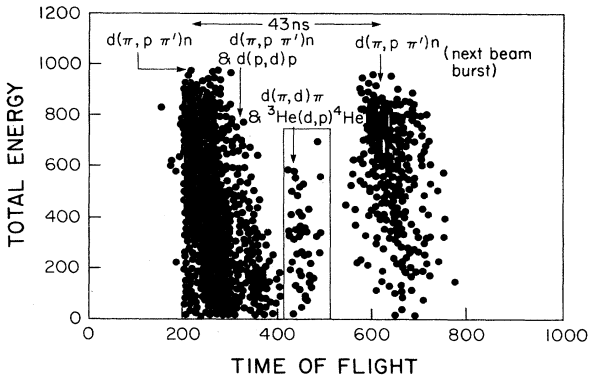

FIG. 11. Time-of-flight at D counter versus total energy in P counter. The ^{3}He$(d,p)^4$He events resulting from elastically scattered deuterons in the LD_2 are enclosed within the box.

ceptance of the system. These stray protons were further reduced by timing the proton signals out at the coincidence gate generated by π·D. A small number of protons were kept in order not to reject higher energy deuterons. The relative timing between the deuterons and protons was adjusted whenever the deuteron angle and/or the beam energy were changed.

Examples of on-line spectra observed during these measurements are displayed in Figs. 7–11. A typical measured pion total energy spectrum is shown in Fig. 7 which clearly shows the separation of elastic from quasifree events. Figure 8 displays ΔE-TOF as detected by the D counter corresponding to the preceding pion spectrum. Figure 9(a) shows the position and angle of these deuterons as measured in the wire chambers $W3$ and $W4$.

As will be discussed in the following section, the energy spectrum of the deuteron plays a very important role in determining t_{20}. For this reason the retractable SSD telescope was used to measure the incident deuteron spectra with good energy resolution and to identify deuterons clearly from other particles. Examples of such measured distributions are shown in Fig. 9(b) which were extracted from plots of energy loss versus total energy such as that shown in Fig. 10 where identified deuterons are enclosed within the box. Runs with the dummy target showed no background in the region of these deuterons. The positional dependence of the deuteron spectrum was studied with the SSD telescope by scanning across the deuteron beam spot. These individual submeasurements were amalgamated appropriately to deduce the complete energy spectra of deuterons arriving at the polarimeter. The thickness of absorber A was adjusted to as to bring the deuteron energy distribution maximally within the calibration range of the polarimeter for each of the t_{20} measurements (20–30 MeV).

Typically, a run consisted of the following series of measurements.

(1) Positioning of the incident pion beam with $W0$.

(2) Selection of the absorber (A) thickness by measuring the actual spectrum of the deuterons with SSD's. The spectra were made to overlap the calibrated efficiency curve maximally.

(3) The two-arm time coincidence gate was adjusted to reject most quasifree πp events.

(4) The deuteron spot was examined with $W3$ and $W4$.

(5) Data was taken. Any interruptions of beam were followed by checks on position with $W0$ as before.

(6) The ^{3}He gas was emptied and backgrounds were investigated using copper foils of an equivalent thickness.

III. ANALYSIS

The general expression for the ^{3}He$(\vec{d},p)^4$He reaction cross section is given by[29]

$$\frac{d\sigma}{d\Omega}(\theta,\phi)=\left[\frac{d\sigma}{d\Omega}(\theta)\right]_0[1+2it_{11}iT_{11}(\theta)\cos\phi+t_{20}T_{20}(\theta)+2t_{21}T_{21}(\theta)\cos\phi+2t_{22}T_{22}(\theta)\cos2\phi]\ , \tag{1}$$

where $[d\sigma/d\Omega(\theta)]_0$ is the unpolarized differential cross section at the proton polar angle θ, and ϕ is the azimuthal angle. The $t_{ij}s$ label the various polarization components of the incident deuterons and the $T_{ij}s$ are the corresponding analyzing powers of the polarimeter. If the polarimeter has cylindrical symmetry then the preceding expression simplifies to

$$\epsilon=\epsilon_0(1+t_{20}T_{20})=\frac{N_p}{N_d}\ , \tag{2}$$

where ϵ is the "efficiency" defined as the ratio of the number of ^{3}He$(d,p)^4$He events (N_p) recorded in the proton telescope to the number of deuterons (N_d) incident on the polarimeter cell, and ϵ_0 is the corresponding

efficiency for unpolarized deuterons. However, the actual measurement of t_{20} involves deuterons arriving at the polarimeter having distributions in position, angle and energy. In Eq. (2) the expression for the efficiency is still valid provided the deuteron distributions retain cylindrical symmetry and are appropriately weighted by the calibration curves. In this case the individual terms $(\epsilon, \epsilon_0, T_{20})$ may be replaced by the averaged quantities $(\bar{\epsilon}, \overline{\epsilon_0}, \overline{T_{20}})$, provided t_{20} is not rapidly changing over the measured range of these experimental parameters. In this case t_{20} is given by

$$t_{20}(T_\pi, \overline{\theta_d^{\text{lab}}}) = \frac{\epsilon(T_\pi, \overline{\theta_d^{\text{lab}}}) - \overline{\epsilon_0}}{\overline{\epsilon_0 T_{20}}} , \tag{3}$$

where $\overline{\epsilon_0}$ and $\overline{\epsilon_0 T_{20}}$ are the quantities calculated from the calibration data using the spatial, angular, and energy spectra at each configuration during the experiment. $\overline{\epsilon_0}$ and $\overline{\epsilon_0 T_{20}}$ are given by

$$\overline{\epsilon_0} = \int N(\nu_j)\epsilon_0(\nu_j) d^5\nu_j \tag{4}$$

and

$$\overline{\epsilon_0 T_{20}} = \int N(\nu_j)\epsilon_0(\nu_j) T_{20}(\nu_j) d^5\nu_j , \tag{5}$$

where $N(\nu_j)$ is the five-dimensional deuteron distribution function ($\nu_j; j = 1-5$ corresponds to the five parameters $(x, y, \theta_x, \theta_y, E)$ which describe the deuteron distribution incident on the polarimeter) for each of the t_{20} measurements normalized to unity:

$$\int N(\nu_j) d^5\nu_j = 1 . \tag{6}$$

Equations (2), (3), and (4) show that the measurements of t_{20} consist, not only of $\epsilon = N_p / N_d$, but also of $N(\nu_j)$. The sign of t_{20} is determined by the difference between the measured ratio of protons to deuterons and the tabulated value of $\overline{\epsilon_0}$ from $N(\nu_j)$. The measurement of ϵ included elimination of backgrounds, counting of deuterons, and identification of valid proton events. The deuteron distribution in position and angle $N(x, y, \theta_x, \theta_y)$ was measured concurrently and TOF spectra provided energy information although its resolution was such that it couldn't be used for analysis purposes. The retractable SSD's measured the energy distributions of the deuterons entering the polarimeter.

For ϵ, the analysis of the data recorded by the computer initially involved examining the signals for each individual detector component and rejecting any events that were inconsistent with an elastic πd signature. The ϵ values could be extracted from the simple ratios of counts in the deuteron and proton telescopes. In this regard, no problems were found in identifying bona fide πd elastic events. However, when processing data from the proton telescope, the selection of $^3\text{He}(d,p)^4\text{He}$ events amongst a large background was a critical factor in the measurement.

The identification of deuterons was made uniquely by considering the TOF vs ΔE signals in the D counter as indicated in Fig. 8. An octagonal cut, shown in the figure, about the elastic deuteron locus was made to select out these events. The information accumulated in the free-running and gated scalers was then used to convert the sampled deuterons within the octagon into a true deuteron count incident on the polarimeter.

The determination of protons from the $^3\text{He}(d,p)^4\text{He}$ reaction was made, primarily, by considering the plot of the TOF signal in the polarimeter D counter versus the total energy deposited in the P counter. Figure 11 shows the various reaction products that were detected. The quasifree protons from the deuterium target were a primary source of background as they would contribute an efficiency of unity while the background in the region of interest had to be kept below 10^{-5}. If any quasifree proton signals remained in the P spectrum after the cut placed on the D counter information, they were easily identified and rejected based on the proton telescope information.

The polarimeter was sensitive to various double-scattering processes since our event detection level was itself at the level of two scattering reactions. The most significant contribution arose from the combination of quasifree protons produced in the LD_2 target through the $d(\pi, p\pi')n$ reaction which subsequently scattered elastically and knocked out deuterons in the target. The TOF of such deuterons fall between the quasifree protons and the elastic deuterons. These were removed by a carefully placed final cut that isolated the true $^3\text{He}(d,p)^4\text{He}$ events as indicated in Fig. 11. These deuterons and the $^3\text{He}(d,p)^4\text{He}$ events tended to merge at higher elastically scattered deuteron energies.

Additional restrictions on the spectra from the P1 counter together with trajectory information from the wire chambers served to remove occasional accidental events and, thus, allowed a clearer separation of (d,p) events. Our success in the complete suppression of these accidental backgrounds is further supported by observing the fact that no events in the time window of the deuterons were seen in succeeding beam bursts (see Fig. 11).

The energy spectrum of the scattered pions in the PIE counter, shown in Fig. 7, highlighted pion peaks associated with elastic deuterons and those from quasifree proton events. These spectra set additional restrictions on the selection of real events especially at higher energies. When we removed the quasifree proton events by altering the timing of the two-arm coincidence, we found that the relative sizes of the two peaks in the PIE spectrum changed accordingly. The raw pion total energy spectrum in Fig. 7 displayed not only the two peaks but also low- and high-energy tails, some of which could also be identified with elastic deuterons in the conjugate arm. Those elastic pions in the low-energy tail came about as a result of scattering (either in the PIE counter or before it) and, subsequently, traversing only a fraction of its anticipated range in the large counter before escaping out through the sides. The energy lost would, therefore, be only a fraction of the total and depend on the geometry of the scattering process. Those in the high-energy tail came about as a result of the "pile up" of signals from the decay of the pion to a muon and subsequently into an electron. Some of these spurious signals were present for several microseconds after the event that produced them and thus contributed in a random fashion to succeeding

TABLE I. Background effects examined with the use of various target materials.

Polarimeter cell	Target cell	Information available
^{3}He	D_2O/H_2O	Backgrounds from the surroundings including oxygen (but subtracted). The effective target thicknesses were made the same as that of the LD_2 target so that all scattering would be the same (initial phase).
^{3}He	Empty	Backgrounds due to other than LD_2.
^{3}He	LH_2	Background check. Check of double scattering processes.
Empty	LD_2	Background protons produced by deuterons, i.e., protons other than ones from the ^{3}He,$(d,p)^4$He reaction
Empty but with a copper foil of equivalent thickness	LD_2	Same as above. Also a check of deuteron contamination in the proton telescope.

events with the effect of apparently increasing the pion energy.

The information available from wire chambers $W1$ and $W2$ supplemented these scintillator measurements. For example, the events corresponding to the low-energy tail in PIE were confirmed as coming about from scattered trajectories. Also, by tracing back to the target we were able to reconstruct the origin of the events in the target and could select a window outside of which the events could be rejected to remove the possibility of quasifree reactions that occurred in the frame of the LD_2 target. Also it was possible to simulate some of the experimental conditions of the previous experiments as discussed later.

Measurements of backgrounds were made by repeating several measurements with different target/polarimeter conditions as indicated in Table I. We found that backgrounds from the LD_2 target were negligible while backgrounds from the empty ^{3}He cell contributed up to 5% of the ^{3}He$(d,p)^4$He count rate for elastically produced deuterons. These arose from stripping reactions in the windows and foils. This background was subtracted from the ^{3}He$(d,p)^4$He events obtained with ^{3}He gas in the cell.

In the measurements of $N(\nu_j)$ in Eqs. (4), (5), and (6), the five parameters $(x,y,\theta_x,\theta_y,E)$ are not totally independent since the deuteron energy depends on the scattering angle at the target which subsequently determines the position and angle of the deuteron incident at the triplet. The triplet, which was adjusted to focus the central rays, would focus different energy deuterons at different positions on the polarimeter. The kinematic spread of the deuteron energy ($\Delta E/E \sim 2\tan\theta\Delta\theta$) was 8% at $\theta_d = 45°$ and 2% at 15° for $\Delta\theta_d = \pm 1.3°$ in our case. This kinematic spread alone is sufficient to break the cylindrical symmetry necessary for the polarimeter to work properly unless the polarimeter is designed to compensate for this effect. In addition, if the five parameters are strongly correlated each must be measured concurrently with the ϵ measurement.

The wire chambers $W3$ and $W4$ were installed based on these reasons. The TOF between the pion and deuteron arms provided the energy information. However, the resolution was not good enough for our analysis purpose so the energy distributions of the deuterons were measured by the retractable SSD telescope before and after each run. While this provided the required energy resolution, it did not furnish its correlation to the other four parameters. To examine this, we scanned the deuteron spectra across the surface of the D counter. It was found that energy distribution was independent of the position on the D counter. This was consistent with the beam optics of the triplet, and was subsequently confirmed by a measurement of the same with a collimator at the entrance of the triplet.

The information gleaned from TOF, $W3$, $W4$, and the measurements mentioned earlier, assured us that it was safe to assume that all the parameters could be treated as independent. The amount of material (target, windows, absorbers, etc.) present between the target and the polarimeter caused significant multiple scattering for deuterons in their path to the polarimeter and destroyed the correlation among themselves.

In this situation we could perform the integration separately over the individual parameters, ignoring correlations. While the dependence of ϵ_0 on the position and angle was not very sensitive, that on the energy distribution was critical and required great care in measurement of the deuteron spectrum and in calculating the value of $\bar{\epsilon}_0$. Equation (4) reduced to

$$\bar{\epsilon}_0 = \int_0^{E_{\max}} N(E)\epsilon_0(E)dE \ , \tag{7}$$

where

$$N(E)=\int N_x(x)N_y(y)N_{\theta_x}(\theta_x)N_{\theta_y}(\theta_y)N_E(E)dx\,dy\,d\theta_x d\theta_y\ , \tag{8}$$

$$\epsilon_0(E)=\int N_x(x)N_y(y)N_{\theta_x}(\theta_x)N_{\theta_y}(\theta_y)N_E(E)\epsilon_0(x,y,\theta_x,\theta_y,E)dx\,dy\,d\theta_x d\theta_y\ . \tag{9}$$

The efficiency curve [Fig. 5(a)] indicates that deuterons with energy ≤ 19 MeV do not contribute to the analyzing reaction, and hence not to ϵ. However, the deuteron detector counted these low-energy deuterons. To account for this we replaced the lower limit in the preceding two integral equations by the threshold energy, $E_{\rm th}$, and corrected the value of ϵ with the fractional difference between $\int_0^{E_{\max}}$ and $\int_{E_{\rm th}}^{E_{\max}}$.

Similarly, the higher-energy tail region (≥ 30 MeV), where the efficiency rises rapidly,[30] must also be treated with due care. Protons produced from these high-energy deuterons were identified by TOF considerations. We ensured (by use of appropriate absorbers) that the maximum contribution from this region to the deuteron/proton counts was not more than 1%. We were unable to get any of the deuteron spectra to fall completely within the flat region of the efficiency curve (25–30 MeV) as had been claimed possible in Refs. 7–9. This is consistent with the view of the broadening of deuteron energy spectra due to the combination of incident pion energy ($\geq 4\%$), kinematic broadening (discussed earlier), and straggling in various materials (approximately 20% of the energy lost). In the case of, say, the $T_\pi = 133$ MeV/$\theta_\pi = 150°$ measurement, we would estimate the broadening to be about 5-MeV FWHM as confirmed by the measurement in Fig. 9(b) (*I*). We note that a direct comparison with the SIN spectra is not possible since they equate these at the center of their cell while we directly measure the spectra at the D counter surface.

The wire chambers surrounding the ^{3}He cell, in principle, enables a simultaneous measurement of the vertical and horizontal asymmetries of the outgoing protons from the (d,p) reaction. From an examination of the expression for the cross section we see that this would allow us to simultaneously extract the values of it_{11}, t_{21}, and t_{22} if the polarimeter were to be appropriately calibrated. The inclusion of wire chambers before and after the ^{3}He cell to measure these asymmetries is an improvement on previous measurements employing a fixed four-leaf configuration of scintillation detectors[30] since corrections could easily be applied for deuteron asymmetries which, if not precisely accounted for, might otherwise greatly distort the extracted values of the observables. At the pion fluxes available in the $M11$ channel the statistical accumulation of ^{3}He$(d,p)^4$He events were too few to apply their use to these asymmetries and so only t_{20} was determined at this time. However, this technique will be in use for the determination of spin-transfer coefficients that are planned in the future.[31]

The analysis of the errors in our data included the statistical and systematic considerations. The general expression that represents the various contributions to each of these errors is given by

$$(\Delta t_{20})^2=\frac{(\Delta\epsilon)^2+(\Delta\overline{\epsilon_0})^2}{(\overline{\epsilon_0 T_{20}})^2}+\frac{(\epsilon-\overline{\epsilon_0})^2(\Delta\overline{\epsilon_0 T_{20}})^2}{(\overline{\epsilon_0 T_{20}})^4}\ . \tag{10}$$

The major source of the statistical errors arises from the proton counting statistics (4–10%) in the πd measurements. Other contributions come from the deuteron counting statistics ($\leq 0.3\%$) and the corresponding calibration errors in $\overline{\epsilon_0}$ and $\epsilon_{T_{20}}$ (6%). The systematic errors, estimated at ~ 0.1, arise predominantly from possible discrepancies between the gain/threshold settings of the polarimeter counters between calibration and their use in the πd measurements ($\sim 5\%$), and also from such factors as the uncertainty in the absolute calibration of the solid-state counters ($\sim 2\%$), and the quantity of analyzing material in the polarimeter ($\sim 1\%$ as determined by pressure and temperature measurements).

TABLE II. Values of $t_{20}^{\rm lab}$ in $\pi^+ d$ elastic scattering.

T_π (MeV)	π^+ flux ($\times 10^7$ s^{-1})	$\Delta p/p$ (%)	$\theta_d^{\rm lab}$ (deg)	$\theta_\pi^{\rm c.m.}$ (deg)	$t_{20}^{\rm lab}$	$\pm\Delta t_{20}^{\rm lab}$
116.0	1.4	2.2	15.0	149.9	−0.07	0.05
125.2	1.6	2.2	15.0	149.8	−0.51	0.11
125.9	2.0	2.2	15.0	149.8	−0.35	0.04
133.4	2.0	2.2	15.0	149.8	−0.71	0.13
			25.0	129.7	−0.55	0.09
			30.0	119.7	−0.56	0.15
139.9	2.2	2.2	15.0	149.8	−0.72	0.11
	3.6	5.0			−0.62	0.11
			18.0	143.8	−0.40	0.07
			25.0	129.7	−0.46	0.07
			30.0	119.7	−0.28	0.04
			35.0	109.7	−0.29	0.05
140.6	2.2	2.2	15.0	149.8	−0.57	0.12
145.4	2.5	2.2	15.0	149.8	−0.58	0.11

IV. RESULTS AND DISCUSSION

Our final t_{20} values are given in Table II and compared in Figs. 12 and 13 with the similar measurements made at SIN and LAMPF, and with some theoretical calculations. Good agreement exists between our data and those of the LAMPF group[3–6] but not with the results of the SIN group. Recently, the tensor analyzing power, T_{20}^{lab}, has been measured[11] at TRIUMF, using a tensor polarized deuterium target. The result of this measurement

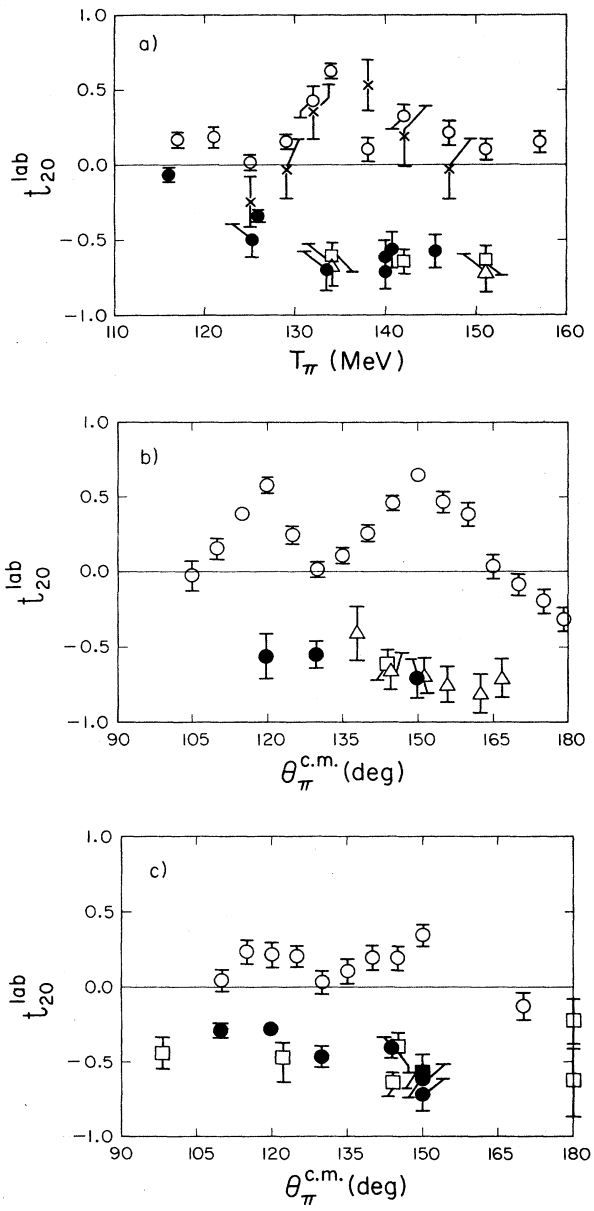

FIG. 12. t_{20} experimental values. The present results are shown with solid circles and square; open circles and crosses are from Refs. 7–9; open squares are from Refs. 3–6; open triangles are from Ref. 11. (a) Excitation curve near $\theta_d^{\text{lab}}=15°$. (b) Angular distribution near 133 MeV. (c) Angular distribution near 140 MeV.

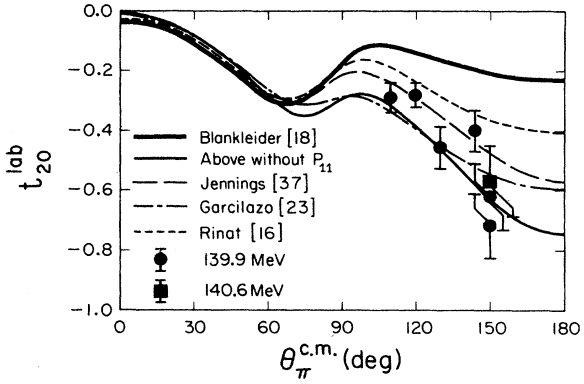

FIG. 13. Comparison of model predictions for t_{20} with our 140 MeV data.

cannot be compared with our result directly since the tensor polarizations measured in our experiment are "laboratory" quantities and in the relation to $t_{20}^{\text{c.m.}}$ they contain other tensor polarization components. On the other hand, the quantity measured in Ref. 11 can be converted directly to the c.m. quantity $T_{20}^{\text{lab}}=T_{20}^{\text{c.m.}}=t_{20}^{\text{c.m.}}$.

In terms of c.m. tensor polarization components, the measured quantity t_{20}^{lab} is given by

$$t_{20}^{\text{lab}}=\tfrac{1}{2}(3\cos\theta-1)t_{20}^{\text{c.m.}} -\sqrt{3/2}\sin 2\theta t_{21}^{\text{c.m.}}+\sqrt{3/2}\sin^2\theta t_{22}^{\text{c.m.}}\ , \tag{11}$$

where θ is the outgoing deuteron laboratory angle.

The sign of the $t_{ij}^{\text{c.m.}}s$ depend on the choice of the quantization axes, i.e., either along the outgoing pion momentum direction or deuteron momentum direction. The relation between the two is given by

$$t_{ij}^{(d)}=(-1)^j t_{ij}^{(\pi)}\ , \tag{12}$$

with most calculated values being given in a system in which the quantization axis is along the pion momentum direction.

In order to compare our result with that of Ref. 11, one must know the values of $t_{21}^{\text{c.m.}}$ and $t_{22}^{\text{c.m.}}$. These have been estimated in three different ways.

(1) Using the full calculation of Blankleider and Afnan.[18]

(2) The same model as above but without the πN P_{11} contribution.

(3) Using amplitudes obtained by fitting the differential cross section, iT_{11}, and t_{20}^{lab}.[25] The contribution from these two quantities to t_{20}^{lab} varied from about 3% to a maximum of 16% depending on the assumption and/or angle. As this is comparable with the measurement uncertainties, we have included the results of Ref. 11 with the t_{20} data shown in Fig. 12. The T_{20} measurements are seen to be in excellent agreement with our (and LAMPF) t_{20} values.

The possible sources(s) of the discrepancy between the results of the SIN group and the other measurements have been investigated in the present experiment. This investigation was possible by the use of information obtained from the wire chambers and the total energy pion detector which were used to simulate some of the experimental conditions of Refs. 3–9 and 30. Our main conclusions are as follows.

(1) The quadrupole triplet was employed to increase the solid angle and to momentum filter particles. While these had been accomplished there were undesirable side effects, among them the kinematic dependence of recoil deuterons on the focusing property of the *QQQ* system. The recoil deuterons emitted from the target had a momentum spread which alone causes the centroid of the deuteron position distribution in the transverse direction to shift several mm at the polarimeter surface. The combined effect of the finite object size (pion beam), kinematic spread, and cross-section difference was such that the centroid of the deuteron distribution in the horizontal direction was shifted ~ 10 mm (right side when viewed from upstream) as measured by wire chambers $W3$ and $W4$ and shown in Fig. 9(a). This is consistent with the predictions of a ray trace program.

In Fig. 9(a) the size of our ^{3}He cell and D counter are indicated by arrows and those used in Refs. 7–9 and 30 are shown by dashed lines. If we were to use a 30-mm diameter ^{3}He cell and a 30 mm deuteron detector, as given in Refs. 7–9 and 30, the effective number of deuterons capable of undergoing the ^{3}He$(d,p)^4$He reaction would be considerably smaller than that detected by the deuteron counter, due to the loss of deuterons by multiple scattering in the aluminum absorbers and the deuteron counter itself, and would result in smaller ϵ values.

The size of the deuteron distribution incident on the polarimeter is dependent on the way in which the triplet was energized. In particular if a 25-mm-diam by 20-cm-long lead cylinder was used at the center of the triplet in order to reduce backgrounds, as in Ref. 30, the effect of the setting of the triplet would be amplified according to our simulation during analysis. Wire chambers $W1$ and $W2$ in front of the pion detectors monitor angular distributions of the scattered pions (hence deuteron angle) within the acceptance of the triplet. By removing the central portions we were able to study the effect of the lead blocker. The normalized position distribution was not significantly affected but the energy distribution as a function of position was affected somewhat such as to make t_{20} more negative. Both the position and energy distributions were more sensitive to small changes in the setting of the triplet. We concluded that in order to avoid the side effects of the employment of the *QQQ* triplet, the ^{3}He cell and the deuteron detector should be as large as possible so that small shifts in the centroid of the deuteron position would not effect the symmetry required for the analysis of t_{20}.

(2) As mentioned earlier, the present experiment consists of two main independent measurements: the efficiency ϵ and the deuteron energy distribution $N(E)$. The distribution function $N(E)$ consists of three parts: those deuterons that never get to the ^{3}He cell but which are detected by the deuteron counter; those deuterons of higher energy whose efficiency and analyzing powers are not known; and those whose energy are within the range of the calibrated efficiency and analyzing power ($19 \leq E \leq 30$ MeV).

The distribution functions $N(E)$ were measured for each run with a SSD telescope having an energy resolution better than 100 keV. The energy absorber thicknesses were so adjusted as to have a maximum overlap between the measured spectra and the ϵ_0 curve shown in Fig. 5(a). Within the limited time available we could only adjust the thicknesses to correspond to distribution centroids that were ± 1.5 MeV of each other and the center of the flat region in the efficiency curve. Examples of spectra measured are shown in Fig. 9(b). Relative to the peak of spectrum I, the position of spectrum II is shifted by -1.5 MeV, and that of spectrum III by -1.0 MeV. For these spectra the tabulated values of $\bar{\epsilon}_0$ as defined in Eq. (4) are 82%, 61%, and 69%, respectively, of the maximum (plateau) value.

If the measured spectrum were to fall entirely within the plateau region of the efficiency curve (25–30 MeV), then $\bar{\epsilon}_0$ would assume the maximum value, and $\epsilon - \bar{\epsilon}_0$ would be more negative (t_{20} more positive). To determine the effect this would have on our data, we combined our ϵ values with a flat region value of $\bar{\epsilon}_0 = 6 \times 10^{-5}$. The results for the $\theta_d^{\rm lab} = 15°$ excitation curve are plotted in Fig. 14. The impression gained in our particular case is one of a prominent structure with a notable discrepancy at 145 MeV, where two independent runs with different absorbers reveal completely different t_{20} values—indicating the extreme sensitivity to the correct application of $\bar{\epsilon}_0$. At 134 MeV, two independent measurements were made (during two separate running periods) using identical absorbers and, as indicated in the figure, they confirm the reproducibility of our data.

Without the energy resolution provided by the SSD telescope, we could not have detected the sensitivity of ϵ_0 to $N(E)$. Not only did the deuteron TOF not provide the required resolution, but also it could not have furnished the effect of the energy absorbers since they were placed

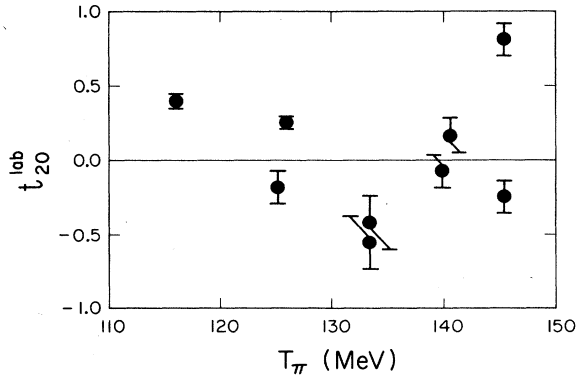

FIG. 14. Resulting effect to our t_{20} values of the incorrect application of the efficiency curve.

in front of the D counter. Had we used TOF information only, our ϵ_0 would also have been constant (plateau value) and our resulting t_{20} values would have appeared as in Fig. 14 and thereafter been interpreted as a "structure." We can conclude that the measurement of $N(E)$ is as important as ϵ, and that the energy distributions must be measured as precisely as possible. It is surmised that the principle cause of the discrepancy between the SIN data and ours stems from the measurement of $N(E)$.

The impact of our results on the present theoretical understanding of the πd elastic system has been to reinforce our belief in the conventional few-body models without the need for introducing such exotic effects as "dibaryon resonances." A comparison with models[12–24] (see Fig. 13) shows general agreement in gross features of the negative sign and lack of any significant structure in the kinematic regions of our measurements. However, these predictions are inadequate for reproducing details of the observables. The failure of theory can be traced to the treatment of the πN P_{11} interaction.

Our data indicates that omitting the P_{11} interaction in the model calculations leads to the best reproduction of experimental data. However to do this, is to ignore the fact that this amplitude is primarily responsible for true pion absorption. The calculated t_{20} values by Garcilazo[22,23] in which in the πN P_{11} input is very small agrees well with our data. Thus the experimental data favors a smaller contribution from the πN P_{11} interaction.

The method adopted by theorists has been to split the πN P_{11} interaction into the repulsive pole (responsible for pion absorption) and attractive nonpole (pion rescattering) terms as shown schematically in Fig. 15. These two terms are needed to take care of sign changes in the P_{11} phase shift at around 150 MeV. However, the exact shape of the repulsive and attractive P_{11} interaction are ambiguous. The individual contributions that these make to the overall P_{11} phase can be rather large but of opposite sign such that they almost cancel out.[32,33]

Garcilazo[23] has provided a detailed explanation of his new relativistic Faddeev theory approach to the πNN system and the refinements to his model calculations. In particular, this model now does form a two-term separable P_{11} potential but with individual pole and nonpole contributions that are considerably smaller than comparative theories, although Lamot *et al.*[15] have subsequently indicated that this does not conserve three-body unitarity. The predictions for t_{20} agree well with our results except at $T_\pi = 134$ MeV, where the data are consistently larger in magnitude by about 1.5 standard deviations. In general, the predictions of this theory for the other πd elastic observables is remarkably good, although the long-standing discrepancies between the measurements and the predictions of large angle $d\sigma/d\Omega$ and the forward angle iT_{11} still remain to be explained.

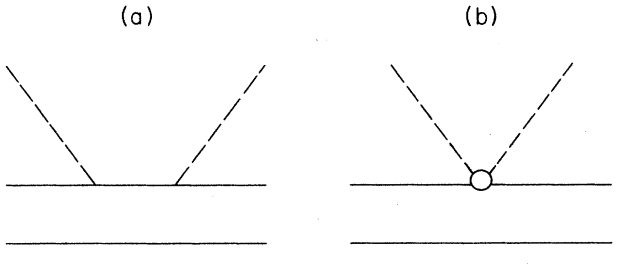

FIG. 15. Decomposition of the P_{11} πN amplitude. (a) The pole term which is mainly responsible for true pion absorption. (b) The nonpole contribution associated with pion rescattering.

Since the pole term includes an intermediate state of two identical fermions, the Pauli exclusion principle would restrict certain contributions from this term in the P_{11} amplitude, and in these partial waves the nonpole term would be expected to dominate. However, the off-shell nature of the absorbing nucleon in the pole term implies that the two nucleons might not be *identical* so the Pauli Principle may only apply in a limited sense.[15,20,23] The extent of this Pauli "blocking" is an interesting question in its own right, and to accurately determine its magnitude will require further measurements, not only of the πd elastic system, but in all the associated and coupled channels together with complimentary phase shift analyses.

The predictions of the model outlined by Afnan and McLeod[20] have been shown to depend very sensitively on the way the P_{11} amplitude is handled. They point out that in the NN-πNN equations the channels other than 0^+, 2^-, 4^-, and 6^- have a three-body channel in which only the nonpole part contributes from the P_{11} due to the Pauli exclusion principle. They concluded that a more fundamental theory and an understanding of the basic πN system is needed to evaluate the extent of the P_{11} splitting and the application of the Pauli principle to the NN^* system.

The recent update by the Lyon group,[15] whose model now includes heavy meson exchanges in the two-body NN sector, provides some indication as to the direction that theories must proceed in order to account for the discrepancies that still exist between predictions and measurements of data. They comment on the inclusion of minor πN partial waves (other than P_{33} and P_{11}) whose importance seems to significantly depend on the energy.

Ferreira and co-workers[34] have examined the effects of short-range Δ-N interactions, not contained in the Faddeev calculations, in terms of a restricted phase shift analysis. They fitted the existing cross-section (total and differential) and iT_{11} data by varying the possible partial-wave contributions of the intermediate Δ-N states which couple to the πd amplitudes of Garcilazo. They conclude that the discrepancies between theoretical predictions and experimental measurements of $d\sigma/d\Omega$ and iT_{11} mentioned earlier can be accounted for in this way. Specifically, incorporating contributions from only the $^5S_2$ and $^5P_3$ partial waves into the amplitude sets of Garcilazo (coupling to $^3P_2$ and $^3D_3$ in πd elastic) seems to reproduce these three observables well at all angles and energies. The predictions for t_{20} also seem to correspond well with the results of our measurements. However, the validity of this approach has yet to be fully tested with other experimental measurements.[31,35,36]

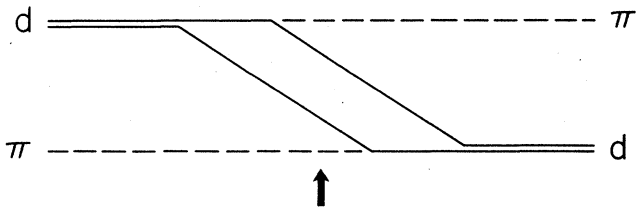

FIG. 16. Additional diagram accounted for in the calculations of Jennings and Rinat in Ref. 37. The arrow indicates the intermediate $\pi\pi NN$ state.

Finally, Jennings, and Rinat[37] have made a detailed analysis of the effect on t_{20} and other observables of contributions arising from diagrams, such as that shown in Fig. 16. Such contributions had previously been ignored since they were expected to be very small (due in part to the existence of the intermediate $\pi\pi NN$ state). The result of adding such diagrams (in the Born Approximation) to the model of Blankleider[18] is shown in Fig. 13. Clearly, the agreement with data is improved.

V. CONCLUSIONS

Our measurements of t_{20} in πd elastic scattering have resolved the discrepancy between previous measurements made at LAMPF[3-6] and at SIN.[7-9] They are consistently negative and show little structure which is in agreement with the LAMPF data and also the recent measurements of T_{20} by Smih *et al.*[11] The results are consistent with the existing few-body theories that have made predictions for this observable[12-24] and remove the need for any exotic effects such as the speculated dibaryon resonances.[9] The SIN results,[7-9] which are so different from all other measurements, could have arisen from the inadequate measurement of the deuteron energy distributions and the oversimplification of the effect of the triplet. The agreement between the polarization measurements, themselves, and the analyzing power measurements,[11] indicates that the polarization measurements are reliable provided that the polarimeter is constructed with care and that proper analyses are undertaken.

Our understanding of how the πN P_{11} amplitude contributes to this interaction has led us to the conclusion that the extent of true pion absorption may have been overestimated in several models that did not correctly account for Pauli blocking. The complete removal of the πN P_{11} potential in most models seems to give the best fit to the experimental data, although this ignores the physical reality of the pion absorption process which predominantly proceeds via the pole term of this intermediate state. Whether this fact implies that Pauli blocking is not applicable to the pole term, or that other factors, such as some partial waves in the Δ-N system, or the inclusion of missing Feymnann diagrams are involved, is not clear at this time.

Blankleider and Afnan[19] have produced a complete set of observable predictions in the πd elastic reaction as well as the coupled channels $\pi d \rightarrow NN$ and $NN \rightarrow NN$. The sensitivity to the P_{11} contribution was examined arriving at the conclusion that, in addition to t_{20}, other observables such as it_{21}^{10}, it_{22}^{10}, it_{20}^{11}, $it_{2\pm1}^{11}$, and $it_{2\pm2}^{11}$ are also strongly dependent on the precise admixing of this amplitude into the model. This has prompted an experimental program to measure these observables[31] and thereby uniquely reconstruct the scattering amplitudes for $\pi d \rightarrow \pi d$.[25] This should provide some clues towards answering the outstanding questions regarding the πN P_{11} amplitude.

ACKNOWLEDGMENTS

This research was supported by grants from the Natural Sciences and Engineering Research Council (Canada) and the National Research Council (Canada) through TRIUMF. The assistance of the TRIUMF and Texas A&M support staff is also greatly appreciated. We gratefully acknowledge the helpful discussions with Dr. B. Blankleider, Dr. I. R. Afnan, Dr. A. S. Rinat, and Dr. B. K. Jennings. In particular we thank Dr. Jennings for making his results available prior to publication.

*Mailing address: TRIUMF, 4004 Wesbrook Mall, Vancouver, B.C., Canada V6T 2A3.
†Present address: Accelerator Laboratory, University of Saskatchewan, Saskatoon, Saskatchewan, Canada S7N 0W0.
‡Present address: University of Saskatchewan, Saskatoon, Saskatchewan, Canada S7N 0W0.

[1]C. R Ottermann *et al.*, Phys. Rev. C **32**, 928 (1985).
[2]G. R. Smith *et al.*, Phys. Rev. C **29**, 2206 (1984).
[3]R. J. Holt *et al.*, Phys. Rev. Lett **43**, 1229 (1979).
[4]R. J. Holt *et al.*, Phys. Rev. Lett. **47**, 472 (1981)
[5]E. Ungricht *et al.*, Phys. Rev. Lett **52**, 333 (1984).
[6]E. Ungricht *et al.*, Phys. Rev. C **31**, 934 (1985).
[7]J. Ulbricht *et al.*, Phys. Rev. Lett. **48**, 311 (1982).
[8]W. Grüebler *et al.*, Phys. Rev. Lett. **49**, 444 (1982).
[9]V. König *et al.*, J Phys. G **9**, L211 (1983)
[10]Y. M. Shin *et al.*, Phys. Rev. Lett. **55**, 2672 (1985).
[11]G. R. Smith *et al.*, Phys. Rev. Lett. **57**, 803 (1986).
[12]W. R. Gibbs, Phys. Rev. C **3**, 1127 (1971).
[13]N. Giraud *et al.*, Phys. Lett. **77B**, 141 (1978); N. Giraud *et al.*, Phys. Rev. C **19**, 465 (1979).
[14]N. Giraud *et al.*, Phys. Rev. C **21**, 1959 (1980).
[15]G. H. Lamot *et al.*, Phys. Rev. C **35**, 239 (1987).
[16]A. S. Rinat *et al.*, Phys. Lett. **80B**, 166 (1979); A. S. Rinat *et al.*, Nucl. Phys. **A329**, 285 (1979).
[17]A. S. Rinat and Y. Starkland, Nucl. Phys. **A397**, 381 (1983).
[18]B. Blankleider and I. R. Afnan, Phys. Rev. C **24**, 1572 (1981).
[19]B. Blankleider and I. R. Afnan, Phys. Rev. C **31**, 1380 (1985).
[20]I. R. Afnan and R. J. McLeod, Phys. Rev. C **31**, 1821 (1985).
[21]M. Betz and T.-S. H. Lee, Phys. Rev. C **23**, 375 (1981).
[22]H. Garcilazo, Phys. Rev. Lett. **53**, 652 (1984).
[23]H. Garcilazo, Phys. Rev. C **35**, 1804 (1987).
[24]T.-S. H. Lee and A. Matsuyama, Phys. Rev. C **36**, 1459 (1987).
[25]N. R. Stevenson and Y. M. Shin, Phys. Rev. C **36**, 1221 (1987).
[26]D. F. Ottewell, TRIUMF internal report.

[27]T. E. Drake *et al.*, Nucl. Instrum. Methods **A265**, 407 (1988).
[28]Y. M. Shin *et al.*, Nucl. Instrum Methods **A274**, 227 (1989).
[29]G. G. Ohlsen, Rep. Prog. Phys. **35**, 717 (1972).
[30]W. Grüebler *et al.*, Nucl. Instrum. Methods **203**, 235 (1982); J. Ulbricht *et al.*, *ibid.* **227**, 57 (1984).
[31]TRIUMF experiment 360 and SIN experiment R-87-04, unpublished.
[32]T. Mizutani *et al.*, Phys. Rev. C **24**, 2633 (1981).
[33]S. Morioka and I. R. Afnan, Phys. Rev. C **26**, 1148 (1982).
[34]F. Pereira and E. Ferreira, J. Phys. G **12**, 1389 (1986); E. Ferreira *et al.*, *ibid.* **13**, L39 (1987); Phys. Rev. C **36**, 1916 (1987).
[35]G. R. Smith *et al.*, Phys. Rev. C **35**, 2343 (1987), and private communication.
[36]C. R. Ottermann, private communication.
[37]B. K. Jennings, Phys. Lett. B **205**, 187 (1988); B. K. Jennings and A. S. Rinat, Nucl. Phys. **A485**, 421 (1988), and private communication.